International Journal of Fatigue 134 (2020) 105428

Contents lists available at ScienceDirect

International Journal of Fatigue

journal homepage: www.elsevier.com/locate/ijfatigue

Technical note

A diagram for capturing and predicting failure locations in notch geometries produced by additive manufacturing

Klas Solberg*, Filippo Berto

Department of Mechanical and Industrial Engineering, Norwegian University of Science and Technology, 7034 Trondheim, Norway

ARTICLE INFO

Keywords:
Failure location
Fatigue
Additive manufacturing
Defects

ABSTRACT

In a recent work by the authors Solberg and Berto (2019), as-built notch geometries of Inconel 718 produced by selective laser melting was investigated under fatigue loading. One of the findings was that fatigue did not initiate from the notch roots, but from defects adjacent. A diagram was developed for capturing the failure locations. Here, a generalized formulation of the diagram is proposed. The model can be useful for developing understanding of which is the dominant feature determining the failure locations; local or global notch geometries. The diagram can be applied in various loading cases, ranging from fatigue to static loading.

1. A diagram for predicting failure location

When dealing with fatigue and fracture of materials and structures, three main questions arise, namely: (1) How much load does it carry? (2) How long does it carry it? And (3) Where does the failure occur? The first two questions are usually emphasized, while the third question remains as a "matter of course". Failure is, of course, occurring in the critical region. So where is this critical region located? At the sharpest notch? At the highest peak stress? At the highest critical distance stress?.

There are many useful criteria capable of predicting failure locations, ranging between brittle and ductile, uniaxial and multiaxial, static and fatigue, local and global. In some cases it is common to report the failure location or the failure mode, this is usually done when dealing with weldments [2], Lattice structures [3], buckling [4] and in general for failure investigations of real structures. One of the reasons for the failure location not being a matter of interest could be the test set-ups (and standardisations of mechanical testing), which are designed for having damage localized in one specific region [5,6]. Another reason could be that it requires effort dealing with the statistics and the variations in the observations, especially if the findings do not support the conclusions of the work.

In the case of additive manufacturing (AM), reporting the failure location can be very useful for understanding the mechanical performance. There are two main reasons:

1. The freedom of design made possible with AM increases the probability of designing complex structures containing notches of different scales, orientations and acuities [3,7–9]
2. The material properties and the manufacturing defects are dependent on the build history, including the geometry of the build [10–14].

Some of the common manufacturing defects in AM are anisotropic microstructure [15,16], residual stresses [17,18], porosity [19], lack-of-fusion [20,21], and high surface roughness [22,23]. In particular, the surface roughness and the amount of defects in the surface region are dependent on the orientation of the surface [12,24]. This means that the combination of complex geometries and manufacturing defects from the process can result in failure initiating from unexpected locations.

Fatigue assessment of AM components is usually done based on manufacturing defects, employing the $\sqrt{area}$-method of Murakami [25]. The defects can be captured either by fractography [26,27] or by computed tomography [28]. In the -method, the location of the defects within the cross-section has to be taken into account. Probabilistic approaches for fatigue assessment has also been developed [29,30]. In particular, the method proposed by Romano et al. is interesting, analysing the location, distribution and size of internal porosity in the presence of notches [29].

In a recent study by the authors [1], it was shown that in as-build AM Inconel 718, fatigue did not initiate from the notch roots in various notch geometries. In Fig. 1a, a polished cross-section of a notched specimen subjected to 2×10^6 cycles is shown. The down-skin surface displays higher surface roughness than the up-skin surface. Fig. 1b shows a fatigue crack initiating from a defect in the down-skin region. A

* Corresponding author.
E-mail address: klas.solberg@ntnu.no (K. Solberg).

https://doi.org/10.1016/j.ijfatigue.2019.105428
Received 24 October 2019; Received in revised form 17 December 2019; Accepted 18 December 2019
Available online 31 December 2019

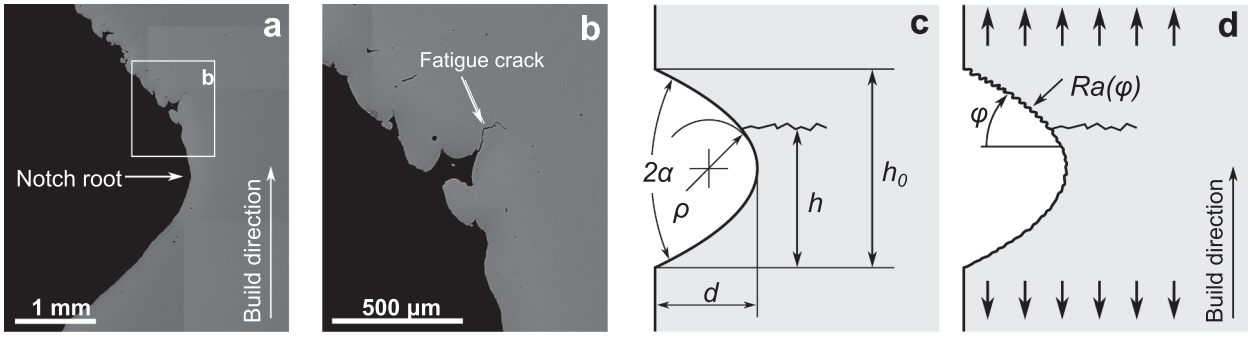

Fig. 1. (a) Cross section of a notch geometry built by AM and subjected to fatigue loading. (b) Detail of a fatigue crack initiating from a defect. (c) Generalized notch geometry with dimensions. (d) Schematic illustration of a notch geometry built by AM, with higher surface roughness in the down-skin surface.

generalized notch geometry is shown in Fig. 1c, and the surface effect generally observed in AM is illustrated in Fig. 1d.

In the work mentioned above, different symmetric double-notched specimen geometries were tested, and the failure locations in the specimens were captured. A brief description of the specimens and some key data are presented in Appendix A; further information can be found in Ref. [1]. Based on the results, a diagram was proposed for capturing the failure location in AM Inconel 718 notch geometries. A schematic illustration of the diagram is shown in Fig. 2a. The vertical axis describes the relative height in the notch, h/h_0, and the horizontal axis is the notch acuity, ξ.

The diagram can be separated into three sections: unnotched, blunt notch and sharp notch. The regions are shaded in Fig. 2a. For a low notch acuity (unnotched) a large scatter in the failure locations were observed; however, on average, the specimens failed from the notch bisector line. Here, the position of the critical defect is controlling the failure location. For a high notch acuity (sharp notch), failure was occurring at the notch root, with a small scatter. In this case, the notch is controlling the failure location. In the intermediate case between unnotched and sharp notch, we have a blunt notch, here the specimen is not failing from the notch root, but from the down-skin region adjacent. This is due to the defects, as shown in Fig. 1a and b.

Based on the design of the specimens in Ref. [1], three competing features controlling the failure location can be identified: (1) Variation in cross-section width (2), macroscopic stress from the notch and (3) the local stress from the defects. In Appendix B, two parametric studies are included; One showing the effect of the macroscopic stresses by varying the notch acuity and one showing the effect of the cross-sectional width for a constant notch acuity.

In this work, an analytical framework for the trend lines in the diagram (Fig. 2a) is proposed, along with some possible applications.

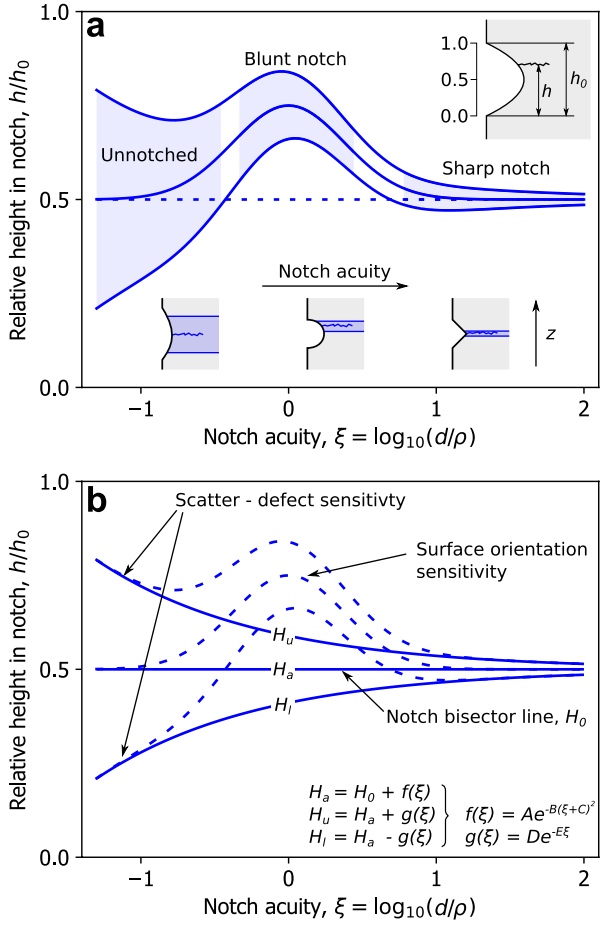

Fig. 2. (a) Schematics of initial diagram developed for AM Inconel 718 from [1]. (b) Generalised diagram and model.

2. Analytical formulation

The diagram compares the notch acuity and location of failure initiation. The notch acuity, ξ, is defined as

$$\xi = \log_{10}(d/\rho). \tag{1}$$

where ρ is the notch radius and d is the notch depth. The notch acuity corresponds to the exponent of the ratio d/ρ *e.g.* $1/1 = 10^0 \Rightarrow \xi = 0$. The location of failure is defined as the relative height in the notch h/h_0, as shown in Fig. 1c.

The diagram and the model are shown in Fig. 2b and consists of three functions; H_a, H_u and H_l, where H_a is the average/mean position of failure, H_u and H_l is the upper and lower predicted positions of the scatter bands based on *e.g.* two standard deviations in failure location. The three functions are defined as

$$H_a = H_0 + f(\xi) \tag{2}$$

$$H_u = H_a + g(\xi) \tag{3}$$

$$H_l = H_a - g(\xi) \tag{4}$$

where

$$f(\xi) = Ae^{-B(\xi+C)^2} \tag{5}$$

$$g(\xi) = De^{-E\xi}. \tag{6}$$

H_0 is the location of the notch bi-sector line, *i.e.* 0.5 for a symmetric notch. $f(\xi)$ describes the roughness-dependence of the surface orientation, *i.e.* $f(\xi)$ is non-zero if the surface roughness is dependent on the build orientation of the surface (which is common in AM metals [23,31,32]). However, if the surface roughness is not dependent on the build orientation $f(\xi)$ is equal to zero. $g(\xi)$ is describing the scatter in

failure locations. It reflects the trend in failure locations occurring with a small scatter for high notch acuity and larger scatter for low notch acuity.

The functions $f(\xi)$ and $g(\xi)$ consists of the parameters: A, B, C, D and E. First considering $f(\xi)$, A is a parameter describing the sensitivity of the build orientation, the height of the perturbation, it should be in the range of 1 and -1. For $A = 0$, there is no sensitivity to the surface orientation, B is describing the width of the perturbation, and C is shifting the location of the peak of the perturbation.

Then $g(\xi)$ is a function describing the scatter of the data or the sensitivity to local defects. D describes the amount of scatter, while E describes the sensitivity to local defects at low notch acuity compared to high notch acuity.

Combining Eqs. (2)–(4) with Eqs. (5) and (6), the formulations yields

$$H_a = H_0 + Ae^{-B(\xi+C)^2} \tag{7}$$

$$H_u = H_0 + Ae^{-B(\xi+C)^2} + De^{-E\xi} \tag{8}$$

$$H_l = H_0 + Ae^{-B(\xi+C)^2} - De^{-E\xi} \tag{9}$$

And gives the diagram as shown in Fig. 2b.

The notch acuity parameter has been altered from the proposed diagram [1]. The eigenvalue exponent based on the notch opening angle of the Lazzarin-Tovo stress field [33] has been removed in order to simplify the model.

Fig. 3 shows the model fitted to the above-mentioned data for AM Inconel 718. The error bars are indicating two standard deviations.

3. Some special cases and applications of the diagram

The diagram and the analytical framework developed here is possible to apply to both empirical data and theoretical values. It can be applied to empirical data from either static of fatigue loading, seeing the scatter and the trends of failure location. Or it can be applied to loading cases where the notch root is not the critical location, *e.g.* the peak stress location under mixed-mode loading. In this section, some of the possible applications of the diagram and the model are shown.

3.1. Surface roughness dependence of surface orientation - additive manufacturing

In the case of AM, the roughness of a surface is dependent on its orientation [31]. *e.g.* down-skin surfaces typically display higher surface roughness than up-skin surfaces. Analytical formulations for connecting the surface roughness to the build orientation has been

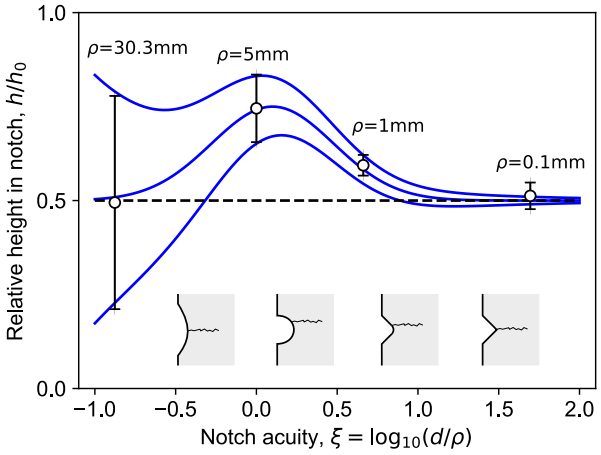

Fig. 3. Model fitted to data from additively manufactured as-built specimens of Inconel 718 [1].

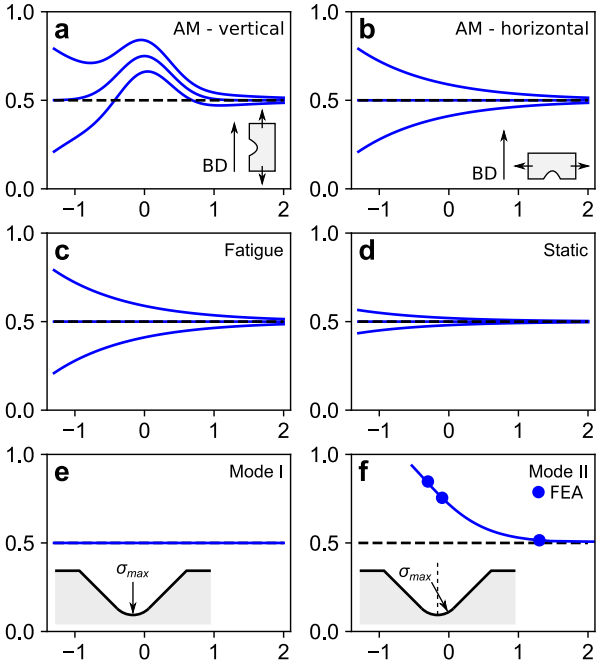

Fig. 4. Possible applications of the diagram. (a) AM built vertically, (b) AM built horizontally, (c) Fatigue loading with surface roughness, (d) static loading with surface roughness, (e) Mode I loading, (f) Mode II loading, verified by FEA.

developed for selective laser melting [31] and fused deposition modelling [32].

Following this, it is possible to make predictions of how the diagram would look for differently orientated specimens subjected to fatigue loading. In Fig. 4a and b, two cases are compared; vertically and horizontally built specimens. The vertically built specimens have highest surface roughness in the down-skin surfaces, and failure is expected to occur from this region in some range of notch geometry. The horizontally built specimens have the highest surface roughness in the notch root. Hence, failure is likely to initiate from this location for all notch acuities. In both cases, the high surface roughness will contribute to generating scatter in the location of failure initiation when dealing with a low notch acuity.

3.2. Static and fatigue loading

In general (not referring to AM), when comparing static and fatigue loading, it should be evident that since fatigue is controlled by localized defects, and are sensitive to sharp notches [34] we expect a high scatter in the failure locations. In the case of static loading, especially for (ductile) engineering materials, the global dimensions are more dominating than the local defects. Hence, less scatter in failure location is expected in the case of static loading than in fatigue.

For a specimen with uniform surface roughness, the general trend for static and fatigue loading is shown in Fig. 4c and d. In static loading, failure will occur close to the minimal cross-section (and notch root), while for fatigue, higher scatter is expected.

3.3. Mixed mode loading

The diagram and the model can be applied to different loading cases, *e.g.* mode I, mode II or mixed-mode loading. In mode I loading the peak stress is located at the notch root. In combinations of mode I and mode II loading, the point of the maximum stress along the edge of the notch does not coincide with the notch root. The location of the peak stress is shifted along the notch edge, according to the ratio between the generalized notch stress intensity factors [35].

The diagram can be employed to compare the different locations of the peak stresses in mode I and mode II loading. For mode I loading, the peak stress is located at the notch root; this is shown in Fig. 4e. For mode II loading a finite element analysis was carried out, capturing the location of the maximum principal stress. A square plate with an opening angle of $2\alpha = 90°$, a constant notch depth and a variable notch radius was considered. Unit displacements were applied according to Lazzarin et al. [36] in order to obtain shear loading. The peak stress was located with an angle of 38°, and the results are plotted in the diagram in Fig. 4f.

4. Conclusions

The work can be summarized by the following points:

- An analytical framework for a diagram connecting failure location to notch acuity has been proposed. The model can fit data on failure initiation site for as-built AM notch geometries subjected to fatigue loading.
- The diagram can increase the understanding of how defects and geometrical features are interacting when dealing with fatigue and fracture behaviour of materials.
- Some applications of the diagram has been demonstrated, both for predictions and for capturing empirical data.

Declaration of Competing Interest

The authors declare that they have no known competing financial interests or personal relationships that could have appeared to influence the work reported in this paper.

Appendix A. Specimen geometries and fatigue data

Fig. A.1a shows the specimen geometries from Ref. [1]. Four different double notched geometries were considered: unnotched, semi-circular, two v-notch with 1 mm radius and v-notch with 0.1 mm radius. The specimens were produced by selective laser melting with a layer height of 50 μm. Fatigue testing was done between 10^4 and 2×10^6 cycles, with a loading ratio of $R = 0$. The fatigue data is shown in Fig. A.1b. Further information about the specimens and the results are available in Ref. [1].

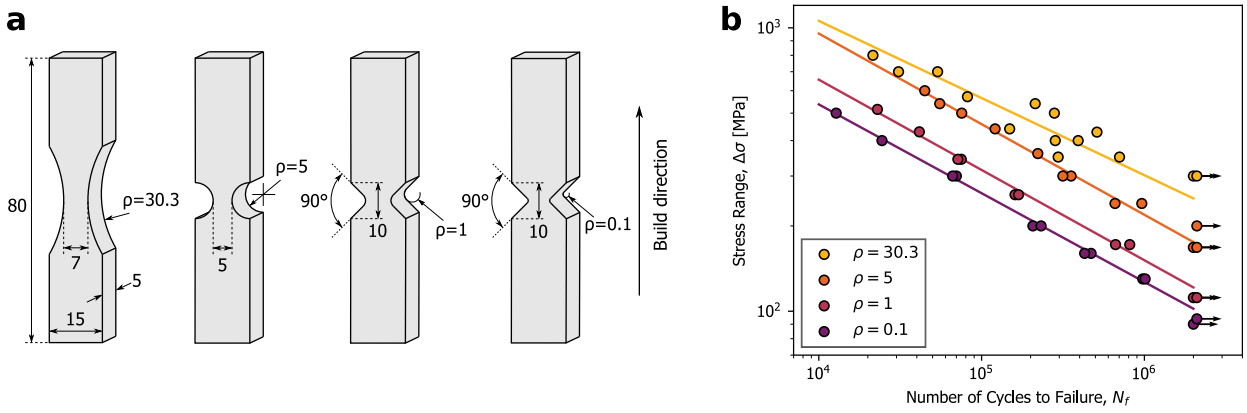

Fig. A.1. (a) Specimen geometries of selective laser melted Inconel 718 and (b) Fatigue data from Ref. [1].

Appendix B. Parametric study of geometric features

In order to understand the influence of the different features of the notch geometries, two parametric studies of the geometric effects were done. In this appendix, we show the geometric effect of the cross-section width and the effect of the notch radius.

Two-dimensional Finite Element Analyses (FEA) were done in Abaqus, using symmetry and applying tension loading. A linear elastic material and CPS8 plane stress elements were used. The maximum principal stress was recorded along the notch edge and normalized with respect to the maximum value for each analysis.

The effect of the cross-sectional width was analysed by considering a semi-circular notch with $\rho = 5$ mm and changing the width from 0.06 mm to 200 mm. This was done in order to see the variations in the stress gradient along the notch edge for different widths. Examples of both narrow and wide cross-section are shown in Fig. B.1a. The normalized stress fields are shown in Fig. B.1b, displaying steep stress gradients for small ligaments and less steep gradients for wide ligaments. Assuming that a defect is present at a certain distance from the notch root, the defects will be more critical if the section is wide, due to the different stress gradients.

Following this logic, a contour plot of the stresses along the free surface was created in Python using cubic interpolation. The contour plot is shown in Fig. B.1c, with the failure locations from the semi-circular specimens inserted. The contour plot shows that for wide cross-sections, the stress fields are stable and not influenced by the width. From the contour plot, it seems that for wide sections, the defects will be critical, while for narrow cross-sections, the cross-section will be the dominant feature.

The effect of the notch radius was investigated based on the v-notched and unnotched specimen geometries. In the FEA-model, a constant width ($w = 5$ mm), notch depth ($d = 5$ mm) and opening angle ($2\alpha = 90°$) was used. The geometry is shown in Fig. B.2a. The normalized stress fields are shown in Fig. B.2b. For small notch radiuses, the stress fields are steep, while for large notch radiuses, the stress fields are less steep. *i.e.* a similar result as in the previous case. A contour plot was generated for the stresses as a function of the notch radius; this is shown in Fig. B.2c. The failure locations of the unnotched and v-notched specimens are inserted, ignoring the variations of the cross-sectional width. The plot in Fig. B.2c shows a similar trend as in Fig. B.1c. A small notch radius gives a steep stress field, indicating failure from the notch tip. For a large notch radius (*i.e.* unnotched) the stress gradient is less steep, and it is expected that the defects are likely to be the dominant feature in failure initiation.

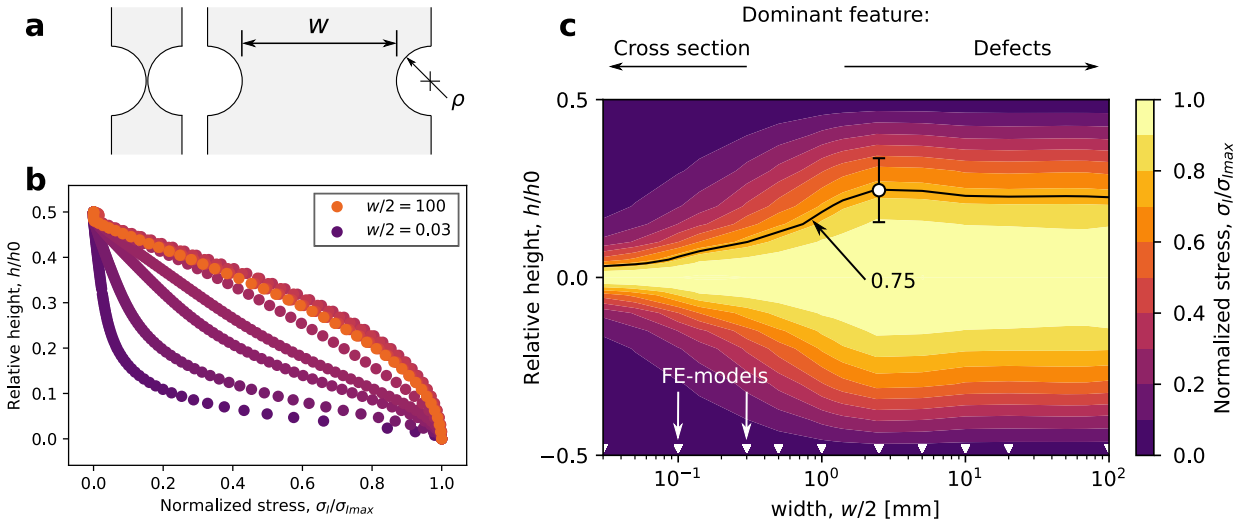

Fig. B.1. Parametric study of specimen width. (a) Example of narrow and wide ligament. (b) Normalized maximum principal stress along the edges of the notches. (c) Contour plot of the stresses along the notch edge for different widths.

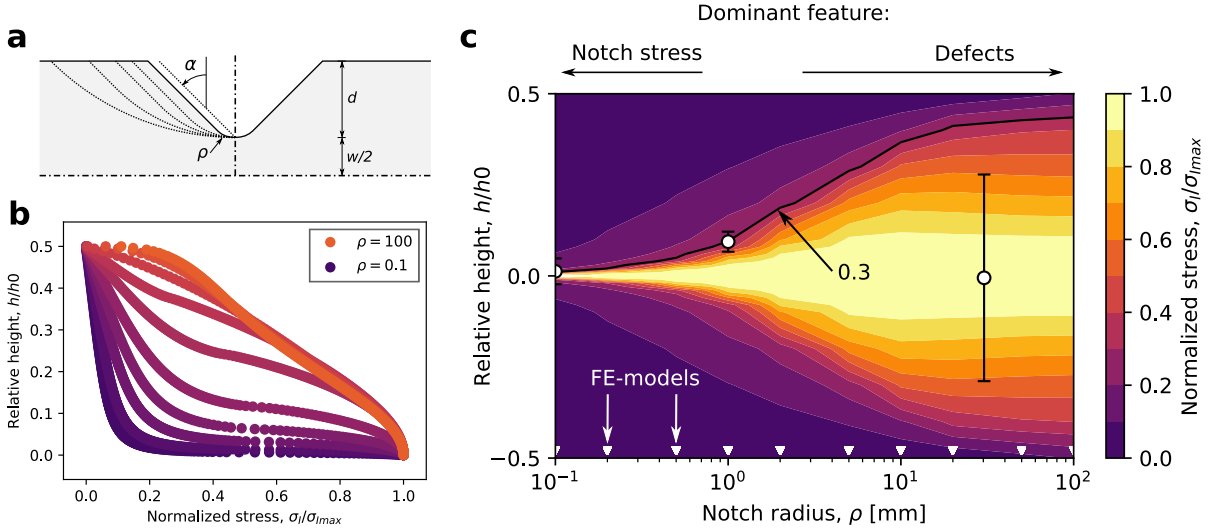

Fig. B.2. Parametric study of notch radius. (a) Different notch radius (b) Normalized maximum principal stress along the edges of the notches. (c) Contour plot of the stresses along the notch edge for different widths.

References

[1] Solberg K, Berto F. Notch-defect interaction in additively manufactured inconel 718. Int J Fatigue 2019;122:35–45.
[2] Somers BR, Pense AW. Welding failure analysis. Mater Charact 1994;33(3):295–309.
[3] Choy SY, Sun C-N, Leong KF, Wei J. Compressive properties of ti-6al-4v lattice structures fabricated by selective laser melting: design, orientation and density. Addit Manuf 2017;16:213–24.
[4] Debski H, Rozylo P, Gliszczynski A, Kubiak T. Numerical models for buckling, postbuckling and failure analysis of pre-damaged thin-walled composite struts subjected to uniform compression. Thin-Walled Struct 2019;139:53–65.
[5] ASTM. E1820-09 standard test method for measurement of fracture toughness, Standard E1820-09. West Conshohocken, PA: ASTM International; 2009.
[6] ASTM. E399-19 standard test method for linear-elastic plane-strain fracture toughness kic of metallic materials, Standard E399-19. West Conshohocken, PA: ASTM International; 2019.
[7] Vyatskikh A, Delalande S, Kudo A, Zhang X, Portela C, Greer J. Additive manufacturing of 3d nano-architected metals. Nat Commun 2018;9:593.
[8] Wauthle R, Vrancken B, Beynaerts B, Jorissen K, Schrooten J, Kruth J-P, et al. Effects of build orientation and heat treatment on the microstructure and mechanical properties of selective laser melted ti6al4v lattice structures. Addit Manuf 2015;5:77–84.
[9] Hussein A, Hao L, Yan C, Everson R, Young P. Advanced lattice support structures for metal additive manufacturing. J Mater Process Technol 2013;213(7):1019–26.
[10] Seifi M, Gorelik M, Waller J, Hrabe N, Shamsaei N, Daniewicz S, et al. Progress towards metal additive manufacturing standardization to support qualification and certification. JOM 2017;69(3):439–55.
[11] Seifi M, Salem A, Satko D, Shaffer J, Lewandowski JJ. Defect distribution and microstructure heterogeneity effects on fracture resistance and fatigue behavior of EBM Ti–6Al–4V. Int J Fatigue 2017;94:263–87.
[12] Yadollahi A, Shamsaei N. Additive manufacturing of fatigue resistant materials: challenges and opportunities. Int J Fatigue 2017;98:14–31.
[13] Hosseini E, Popovich V. A review of mechanical properties of additively manufactured inconel 718. Addit Manuf 2019;30:100877.
[14] Tammas-Williams S, Todd I. Design for additive manufacturing with site-specific properties in metals and alloys. Scripta Mater 2017;135:105–10.
[15] Kok Y, Tan X, Wang P, Nai M, Loh N, Liu E, et al. Anisotropy and heterogeneity of microstructure and mechanical properties in metal additive manufacturing: a critical review. Mater Des 2018;139:565–86.
[16] Lewandowski JJ, Seifi M. Metal additive manufacturing: a review of mechanical properties. Annu Rev Mater Res 2016;46(1):151–86.
[17] Mukherjee T, Zhang W, DebRoy T. An improved prediction of residual stresses and distortion in additive manufacturing. Comput Mater Sci 2017;126:360–72.
[18] Megahed M, Mindt H-W, N'Dri N, Duan H, Desmaison O. Metal additive-manufacturing process and residual stress modeling. Integr Mater Manuf Innov 2016;5(1):61–93.
[19] Hojjatzadeh S, Parab N, Yan W, Guo Q, Xiong L, Zhao C, et al. Pore elimination mechanisms during 3d printing of metals. Nat Commun 2019;10:3088.
[20] Mukherjee T, DebRoy T. Mitigation of lack of fusion defects in powder bed fusion additive manufacturing. J Manuf Process 2018;36:442–9.

[21] Coeck S, Bisht M, Plas J, Verbist F. Prediction of lack of fusion porosity in selective laser melting based on melt pool monitoring data. Addit Manuf 2019;25:347–56.
[22] Balachandramurthi AR, Moverare J, Dixit N, Pederson R. Influence of defects and as-built surface roughness on fatigue properties of additively manufactured alloy 718. Mater Sci Eng A 2018;735:463–74.
[23] Pegues J, Roach M, Williamson RS, Shamsaei N. Surface roughness effects on the fatigue strength of additively manufactured Ti-6Al-4V. Int J Fatigue 2018;116:543–52.
[24] Li P, Warner D, Pegues J, Roach M, Shamsaei N, Phan N. Towards predicting differences in fatigue performance of laser powder bed fused Ti-6Al-4V coupons from the same build. Int J Fatigue 2019;126:284–96.
[25] Murakami Y. Stress concentration. In: Murakami Y, editor. Metal fatigue. Oxford: Elsevier Science Ltd; 2002. p. 11–24 [chapter 2].
[26] Meneghetti G, Rigon D, Gennari C. An analysis of defects influence on axial fatigue strength of maraging steel specimens produced by additive manufacturing. Int J Fatigue 2019;118:54–64.
[27] Gunther J, Krewerth D, Lippmann T, Leuders S, Troster T, Weidner A, et al. Fatigue life of additively manufactured Ti–6Al–4V in the very high cycle fatigue regime. Int J Fatigue 2017;94:236–45.
[28] Solberg K, Guan S, Razavi SMJ, Welo T, Chan KC, Berto F. Fatigue of additively manufactured 316l stainless steel: the influence of porosity and surface roughness. Fatigue Fract Eng Mater Struct 2019;42(9):2043–52.
[29] Romano S, Bruckner-Foit A, Brandao A, Gumpinger J, Ghidini T, Beretta S. Fatigue properties of AlSi10Mg obtained by additive manufacturing: defect-based modelling and prediction of fatigue strength. Eng Fract Mech 2018;187:165–89.
[30] Yates JR, Efthymiadis P, Antonysamy AA, Pinna C, Tong J. Do additive manufactured parts deserve better? Fatigue Fract Eng Mater Struct 2019;42(9):2146–54.
[31] Strano G, Hao L, Everson RM, Evans KE. Surface roughness analysis, modelling and prediction in selective laser melting. J Mater Process Technol 2013;213(4):589–97.
[32] Rahmati S, Vahabli E. Evaluation of analytical modeling for improvement of surface roughness of fdm test part using measurement results. Int J Adv Manuf Technol 2015;79(5):823–9.
[33] Lazzarin P, Tovo R. A unified approach to the evaluation of linear elastic stress fields in the neighborhood of cracks and notches. Int J Fract 1996;78:3–19.
[34] Atzori B, Lazzarin P. Notch sensitivity and defect sensitivity under fatigue loading: two sides of the same medal. Int J Fract 2001;107(1):1–8.
[35] Berto F, Lazzarin P. Recent developments in brittle and quasi-brittle failure assessment of engineering materials by means of local approaches. Mater Sci Eng: R: Rep 2014;75:1–48.
[36] Lazzarin P, Zappalorto M, Berto F. Generalised stress intensity factors for rounded notches in plates under in-plane shear loading. Int J Fract 2011;170(2):123.